Theory of tunneling across hydrogen-bonded base pairs for DNA recognition and sequencing

Myeong H. Lee and Otto F. Sankey
Department of Physics, Arizona State University, Tempe, Arizona 85287-1504, USA
(Received 12 February 2009; published 18 May 2009)

We present the results of first-principles calculations for the electron tunnel current through hydrogen-bonded DNA base pairs and for (deoxy)nucleoside-nucleobase pairs. Electron current signals either through a base pair or through a deoxynucleoside-nucleobase pair are a potential mechanism for recognition or identification of the DNA base on a single-stranded DNA polymer. Four hydrogen-bonded complexes are considered: guanine-cytosine, diaminoadenine-thymine, adenine-thymine, and guanine-thymine. First, the electron tunneling properties are examined through their complex band structure (CBS) and the metal contact's Fermi-level alignment. For gold contacts, the metal Fermi level lies near the highest occupied molecular orbital for all DNA base pairs. The decay constant determined by the complex band structure at the gold Fermi level shows that tunnel current decays more slowly for base pairs with three hydrogen bonds (guanine-cytosine and diaminoadenine-thymine) than for base pairs with two hydrogen bonds (adenine-thymine and guanine-thymine). The decay length and its dependence on hydrogen-bond length are examined. Second, the conductance is computed using density functional theory Green's-function scattering methods and these results agree with estimates made from the tunneling decay constant obtained from the CBS. Changing from a base pair to a deoxynucleoside-nucleobase complex shows a significant decrease in conductance. It also becomes difficult to distinguish the current signal by only the number of hydrogen bonds.

DOI: 10.1103/PhysRevE.79.051911 PACS number(s): 87.14.gk, 72.80.−r, 73.23.Hk

I. INTRODUCTION

There has been much research on charge transfer in DNA due to potential applications such as a molecular wire in a mesoscopic electronic device [1] or in sequencing technology [2]. Most studies on conduction have been focused on π stacking where charge transfer occurs along the DNA strand. Charge transfer in DNA along the backbone axis occurs as either oxidative hole transfer or reductive electron transfer. Fink and Schönenberger [3] measured directly the electrical current across a few DNA molecules, and argued that DNA is ideally suited for the construction of mesoscopic electronic devices. Porath *et al.* [4] measured the current through the double-stranded polyguanine-polycytosine [poly(G)-poly(C)] DNA molecules connected to the two metal electrodes, and showed that DNA conducts charge and behaves in the same way as the silicon-based semiconductor. Spectroscopic measurements of photoinduced electron transfer in synthetic DNA were performed by Lewis *et al.* [5]. Xu *et al.* [6] measured conductance of single DNA molecules in aqueous solutions, and showed that the tunneling decay along DNA is much less rapid than in alkanes. A theoretical hopping model for charge migration in DNA was proposed by Berlin *et al.* [7] and Grozema *et al.* [8].

There is recent interest in sequencing DNA by a charge-transfer mechanism, and a variety of schemes have been proposed. It has been proposed to identify the DNA base by measuring the ionic current when the DNA translocates a nanopore [9–12]. Direct charge transfer within DNA but across the backbone axis has attracted attention for the purpose of DNA sequencing. An initial theoretical study carried out by Zwolak and Di Ventra [13] where tunneling occurred across DNA showed that each nucleotide has a unique electrical signature, providing the possibility of sequencing DNA by measuring the transverse current when single-stranded DNA translocates a nanopore. However, Zikic *et al.* [14] reported that the geometrical fluctuations of the bases within the nanoelectrodes dominate the current signature, suggesting that it is impossible to sequence DNA by just measuring the transverse current.

The coupling interaction between a base pair is the hydrogen bond. Ohshiro and Umezawa [15] showed that electron tunneling is much facilitated when the hydrogen bond is formed between a Watson-Crick complementary base pair compared to a noncomplementary base pair. He *et al.* [16] took this idea further and demonstrated the feasibility of electrically reading a DNA base pair. They measured the tunnel current when the nucleobase-functionalized scanning tunneling microscope (STM) tip is pulled away from a deoxynucleoside monolayer. It was shown that the tunnel current decays more slowly in a complementary Watson-Crick base pair (G-C) compared to the G-T wobble base pair [16]. Furthermore they proposed a new sequencing scheme of native DNA with hydrogen-bond-mediated molecular recognition [17].

In this paper we report the electron-tunneling properties of hydrogen-bonded DNA base pairs in the transverse direction by first-principles calculation. Our work is motivated by the experimental work which observes an enhanced tunnel current for a complementary DNA base pair [15–17]. We explore the possibility of distinguishing the DNA base pairs using the tunnel current across a DNA base pair in the direction perpendicular to the backbone axis with the goal of (i) obtaining a better understanding of the DNA recognition and sequencing studies, (ii) determining whether complementary base pairs [G-C and adenine-thymine (A-T)] conduct better than wobble base pair (G-T), and (iii) whether the number of hydrogen bonds involved in base pairing produces significant differences in conductance. We also examine the effect of adding deoxyribose to one nucleobase, which is explored in recent STM experiments by He *et al.* [16].

Key to the tunneling signature in base pairing is the hydrogen bond. A-T base pairs have two hydrogen bonds, while G-C base pair has three hydrogen bonds. We investigate the role of the hydrogen bond on electronic transport through DNA base pairs in several different ways. First, we study the effect of the number of hydrogen bonds in the base pair by artificially modifying the bases. We also study the 2-aminoadenine–thymine (2AA-T) base pair. 2AA is a derivative of adenine and is able to form three hydrogen bonds with thymine [18,19]. Second, we obtain a quantitative global view of electron tunneling through base pairs by exploring their complex band structure (CBS). We also determine the current-voltage (*I-V*) curve for each base pair using Green's-function scattering theory. Finally, the effect of the deoxyribose and the effect of lengthening the hydrogen bonds are determined.

Previous theoretical studies have been reported on the electron-transport properties through some DNA base pairs. The current-voltage dependence and conductance spectrum were calculated using semiempirical nonequilibrium Green's function for adenine-thymine DNA base pair sandwiched between Au contacts, and significant conductance at small voltage biases was reported [20]. Effect of protonation on the electronic properties of the DNA base pairs (G-C, A-T, and A-A base pairs) was found to be different for different base pairs by computing the transmission function of each DNA base pair at different bias voltages [21]. Jauregui and Seminario [22] calculated the electrical characteristics of Watson-Crick and non-Watson-Crick base pairs using a density-functional theory (DFT) and Green's function. They found that the C-G base pair is a better electron conductor than the A-T in the range of −1 to 1 V bias and different base pairs exhibit distinct *I-V* characteristics which can be used for detecting or sequencing DNA.

An outline of this paper follows. The DNA base pairs explored in this paper are three Watson-Crick complementary base pairs of G-C, A-T, and 2AA-T and one wobble base pair of G-T. In Sec. II we describe the structures of the DNA base pairs. In Sec. III we determine the exponential decay constant as an electron tunnels through the DNA base pair by computing the CBS. The CBS gives a global view, for all energy electrons, of the conduction properties inherent to the molecular system [23]. The complex band structure however does not include the effects of metal-molecule interaction at the contact interface. An estimate of tunnel conductance of each DNA base pair is made using the maximum decay constant, and so gives the "worst-case scenario" possible for any metal contact. In Sec. IV we determine the alignment of the Fermi level relative to the highest occupied molecular orbital (HOMO) for gold contacts. Coupling this electron energy with the CBS tunneling decay allows a simple estimate of conductance to be determined specifically for gold contacts. Gold contacts were used in the experiments of He *et al.* [16,17]. In Sec. V we perform scattering theory calculations of *I-V* characteristics and independently check conductances and the Fermi-level alignment, and determine the transmission function through base pairs. In Sec. VI we determine the *I-V* curve for hydrogen-bonded deoxynucleoside-nucleobase complex. In Sec. VII, the effect of the number of hydrogen bonds on the conductance is examined. The relationship between hydrogen-bond distance and conductance decay rate is discussed in Sec. VIII. In Sec. IX, we summarize our conclusions.

II. GEOMETRY OF BASE PAIRS

All the DNA bases (C, G, A, and T) and base pairs (G-C, A-T, G-T, and 2AA-T) were relaxed to have a minimum energy in vacuum using a quantum chemistry code (GAMESS) [24] with the 6-31+G(d,p) basis using density-functional theory. The "best" exchange-correlation functional for weakly bound systems (van der Waals or hydrogen-bond interactions) is an issue. Tsuzuki and Lüthi [25] showed that PW91 performs best in terms of interaction energies. Studies on the hydrogen-bond length and bond energy of DNA base pairs [26–33] show that A-T Watson-Crick base pair shows good agreement with experiment, while G-C base pair is not as good [28,31,32]. However, B3LYP [35] shows less mean absolute deviation in hydrogen-bond length from experiment [34]. van der Wijst *et al.* [32] showed the mean deviations to be 0.067 Å for B3LYP and 0.087 Å for PW91. However, they also showed that BP86 [57] and PW91 [58] perform better for both the hydrogen-bond length and bond energy of

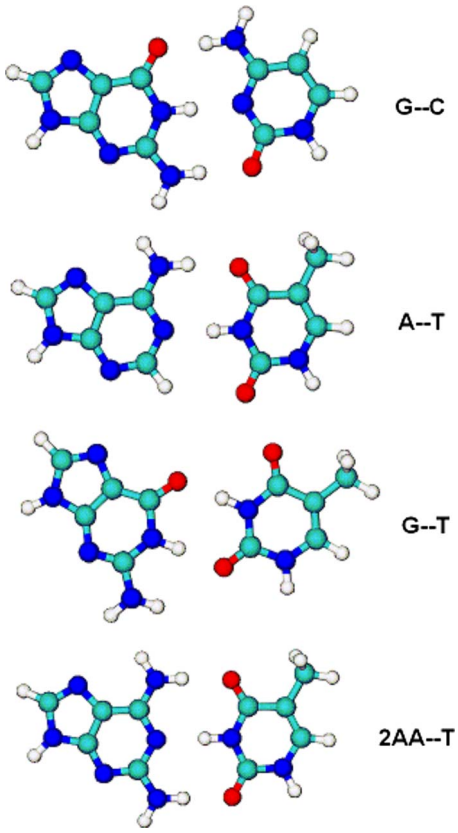

FIG. 1. (Color online) Relaxed structures of G-C, A-T, G-T, and 2AA-T base pairs. A derivative of adenine (2AA or diaminoadenine) is used to make three hydrogen bonds with thymine. The hydrogen-bond distances (H-*X* or *X*-H) were 1.745, 1.891, and 1.911 Å from top to bottom for G-C; 1.886 and 1.837 Å for A-T; 1.763 and 1.816 Å for G-T; and 1.937, 1.892, and 1.939 Å for 2AA-T. All the base pairs are aligned in plane after optimization.

TABLE I. Hydrogen-bond lengths in Å for A-T and G-C. The last row lists the values obtained in this work. The results from others and from experiment are also shown.

	A-T		G-C		
Method	NH···O	N···HN	O···HN	NH···N	NH···O
X ray[a]	2.95	2.82	2.91	2.95	2.86
RI-MP2/cc-pVTZ[b]	2.86	2.83	2.75	2.90	2.89
MP2/6-31G* [c]	2.99	2.88	2.84	2.97	2.95
MP2/6-31G** [c]	2.97	2.84	2.81	2.94	2.93
HF/cc-pVTZ(-f)[d]	3.06	2.92	2.83	2.95	2.92
HF/6-31G** [e]	3.09	2.99	2.92	3.04	3.02
BP86/TZ2P[f]	2.85	2.81	2.73	2.88	2.87
BP86/cc-pVTZ[g]	2.87	2.83	2.73	2.90	2.89
PBE/TZ2P[g]	2.87	2.80	2.73	2.89	2.87
PW91/TZ2P[g]	2.85	2.79	2.72	2.88	2.86
B3LYP/cc-pVTZ[g]	2.93	2.88	2.79	2.94	2.93
B3LYP/6-31G** (this work)	2.90	2.89	2.78	2.93	2.93

[a]Saenger [34].
[b]Šponer *et al.* [29].
[c]Mo [31].
[d]Brameld *et al.* [26].
[e]Šponer *et al.* [30].
[f]Guerra *et al.* [27].
[g]van der Wijst *et al.* [32].

A-T and G-C base-pair systems with water molecules and counterions. Our model of electron transport does not include water or counterions. Here we choose B3LYP for geometry optimization because the hydrogen-bond length is the more relevant issue concerning tunneling.

All the base pairs are aligned in plane after optimization. The optimized structures are shown in Fig. 1. The hydrogen-bond lengths are shown in Tables I and II. Results from others are also shown for A-T and G-C. The hydrogen-bond distance that we obtained shows good agreement with similar calculations from others. Note that the three-hydrogen-bonded 2AA-T complex has slightly increased hydrogen-bond lengths compared to the two-hydrogen-bonded A-T base pair (1.89 Å→1.94 Å, 1.84 Å→1.89 Å). The hydrogen-bond length for the third hydrogen bond is 1.94 Å.

The electron energy levels for each nucleobase obtained using the same quantum chemistry code [24] using B3LYP show that all the nucleobases have similar band gaps (~5 eV) between HOMO and lowest unoccupied molecular orbital (LUMO) [Fig. 2(a)]. Experimentally, the nucleobases have band gaps ranging from 4.3 to 4.7 eV [36–39]. Standard density-functional theory is a ground-state theory and there are errors in predicting band gaps since they involve excited states. In some cases simpler models can give better results [40]. Guanine has the highest energy level for the HOMO and LUMO. Figure 2(b) illustrates how the band gap changes when two isolated nucleobases (C and G) are brought together to form hydrogen bonds. The band gap decreases compared to the isolated nucleobases—the HOMO and the LUMO for G-C base pair are dominated by the orbitals from guanine and cytosine, respectively.

TABLE II. Hydrogen-bond lengths in Å for 2AA-T and G-T.

	2AA-T			G-T	
Method	NH···O	N···HN	NH···O	O···HN	NH···O
B3LYP/6-31G**	2.95	2.94	2.96	2.80	2.84

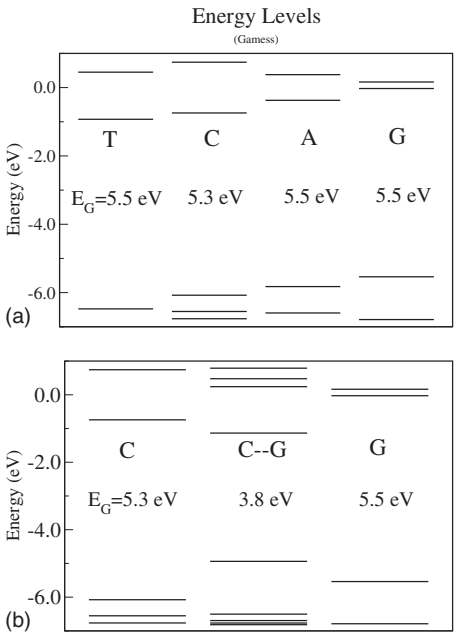

FIG. 2. Energy-level diagrams for (a) DNA bases (T, C, A, and G) and (b) the base pair (C-G). Guanine has the highest energy levels for the HOMO and LUMO, and thymine has the lowest energy levels for the HOMO and LUMO. The band gap between HOMO and LUMO levels decreases as the two bases (C and G) form a base pair (C-G).

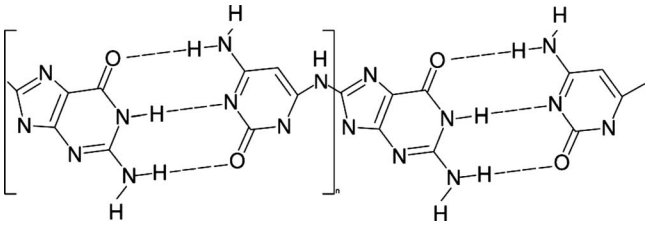

FIG. 3. Schematic diagram of a periodic structure for the G-C base pair. Two unit cells are shown. Hydrogen atoms at either end are removed and replaced with a linker -NH- to connect each unit cell.

III. COMPLEX BAND STRUCTURE AND DECAY CONSTANT

The complex band structure is the extension of the conventional real band structure to complex Bloch k vectors. It gives the insight into the inherent conduction properties of the molecule without reference to which metal contact is used. The tunneling properties at all energies are determined in this way rather than just at the energy of the metal's Fermi level. To accomplish this an artificial periodic system must be formed. A periodic system has electron Bloch energy eigenstates, $\psi(x)=e^{ikx}u(x)$, where $u(x)$ has the lattice periodicity. For an infinitely long periodic system, only real Bloch wave vectors k are allowed since the wave function will blow up at $x=\pm\infty$. Complex k vectors are solutions to Schrödinger's equation and are allowable when the system has finite size as in a molecule. The imaginary part of the wave vector describes the evanescent tunneling states. The electron-tunneling probability decreases as $e^{-\beta L}$, where $\beta=2\times\mathrm{Im}[k]$ and L is the length of the molecule. This evaluation of $\beta(E)$ is the molecular replacement of an electron of energy E tunneling through a square well of height V_0 given by $\beta(E)=2\sqrt{2m(V_0-E)/\hbar^2}$. The square well is an analogy, and no value of V_0 is needed in the present theory. Information on the potential-energy function is contained in the Hamiltonian and β in the complex-band-structure formalism takes this into account naturally. A simple estimate of the conductance [41] G follows from $\beta(E)$, $G=G_0e^{-\beta(E)L}$, where G_0 is the quantum of conductance ($G_0=77\ \mu$S).

The complex band structure was computed within DFT in the local-density approximation (LDA) with ultrasoft pseudopotentials [42] using a plane-wave basis set [43]. The plane-wave basis set and LDA (Slater/PZ) exchange-correlation functional were used. The allowed values of complex k are determined for a given energy E (rather than k determining E). We construct an artificial periodic base-pair polymer to perform the analysis. Hydrogen atoms on either end of a base pair are removed and each unit is connected to neighbors on either side using a linker (-NH-). Figure 3 shows the schematic diagram of periodic structure for the G-C base pair with two unit cells shown.

Figures 4(a)–4(d) show the complex band structures of (a) G-C, (b) A-T, (c) G-T, and (d) 2AA-T base pairs. The energy levels are adjusted so that the HOMO is zero energy. The real-k bands (left panel) are very flat because there is little interaction between the neighboring unit cells. The decay parameter $\beta(E)$ (related to the imaginary part of the k vector)

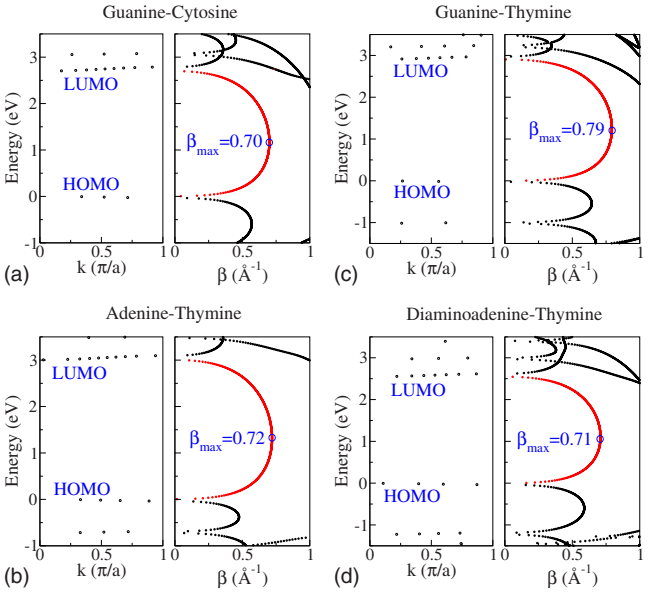

FIG. 4. (Color online) Complex band structures of (a) G-C, (b) A-T, (c) G-T, and (d) 2AA-T base pairs. The conventional band structure with real k is shown in left panel, and the decay constant β (defined as $2\times\mathrm{Im}[k]$) is plotted in the right panel. The semielliptical curve connecting the HOMO and LUMO levels of the conventional band structure (shown in red) is the most penetrating state in the band-gap region. The decay constant β_{max} occurs when the Fermi level lies near the middle of the band gap.

is shown on the right panel. We focus primarily on the energy region between the HOMO and the LUMO since the metal Fermi level typically lies between them. (As we will see later, for gold it lies just above the HOMO.)

The real band structure [Fig. 4(a)] of the G-C base pair shows that the band gap E_G of G-C is 2.70 eV at $k=0$. This band gap is smaller than that obtained in Sec. II for the isolated G-C base pair [$E_G=3.80$ eV; Fig. 2(b)]. The main reason for this is the difference in the exchange/correlation potential, although there is a small effect due to periodicity. The β branch within the band-gap region appears as a semielliptical curve [shown in red in Fig. 4(a)]. The maximum value of β (β_{max}) on the semielliptical curve gives the maximum spatial decay rate of the tunneling probability and the minimum electrical conductivity of the molecule. This occurs when the Fermi level of the metal lies at the energy of β_{max}. An estimate of the minimum conductance of the base pair of length L (the length of the periodic unit cell is used here) can be estimated as $G_{min}=G_0e^{-\beta_{max}L}$.

A summary of the complex-band-structure results for G-C, A-T, G-T, and 2AA-T base pairs is shown in Table III. Listed are the band gaps (E_G), the unit-cell lengths (L), and the maximum values of the decay constant (β_{max}). Of prime importance are the electrical conductances. Listed are the minimum estimated conductances [$G(\beta_{max})$] using β_{max}, an estimated conductance for gold contacts by using the energy of the computed gold/molecule Fermi-level alignment (Sec. IV), and using $\beta(E_F)$, and finally the results from an independent Green's-function I-V calculation (Sec. V) which does not rely on complex band structures.

There are several features to notice from the complex-band-structure calculation results. First, the decay constant of

TABLE III. The band gaps (E_G), unit-cell lengths (L), and the maximum decay constants near midgap (β_{max}) for GC, A-T, G-T, and 2AA-T. The systems with two hydrogen bonds and three hydrogen bonds are denoted as 2H and 3H, respectively. The estimated minimum conductance [$G_{min}(\beta_{max})$] is obtained by using the maximum β. For the special case of gold contacts, the estimate [$G_{Est}(\beta(E_F))$] uses the decay constant at the gold Fermi level. The estimated conductances are compared with Green's-function I-V calculation of the conductance ($G_{I\text{-}V}$) of a base pair sandwiched between gold slab electrodes.

Base pair	E_G (eV)	L (Å)	β_{max} (Å^{-1})	$G_{min}(\beta_{max})$ (nS)	$\beta(E_F)$ (Å^{-1})	$G_{Est}(\beta(E_F))$ (nS)	$G_{I\text{-}V}$ (nS)
G-C (3H)	2.70	12.8	0.70	9.82	0.35	870	83.8
A-T (2H)	3.01	12.8	0.72	7.83	0.47	180	22.2
G-T (2H)	2.91	12.5	0.79	3.70	0.48	190	23.7
2AA-T (3H)	2.56	12.8	0.71	8.87	0.30	1770	119

the hydrogen-bonded base pair in the midgap region (β_{max}) is about 0.70 Å^{-1} for all but the wobble base pair G-T, which is 0.79 Å^{-1}. These values are comparable to decay in a σ-bonded system (e.g., 0.79 Å^{-1} for alkane chain [41,44]). The value of β_{max} is considerably higher than typical values of β for π-bonded linked-ring system (~0.2–0.5 Å^{-1}) [45]. Not unexpectedly, this result shows that the hydrogen bond connecting the base pair contributes to an increase in β, the base-pair decay constant is a some quantum-mechanical "average" of a small decay through π-bonded bases and the more rapid decay through the weak hydrogen bond.

A second feature is that the decay constant (β_{max}) shows only a slight difference between the base pairs even between pairs with different numbers of hydrogen bonds. The complementary base pairs (G-C and 2AA-T) with three hydrogen bonds have the smallest value of β_{max} (0.70 and 0.71 Å^{-1} respectively). Note that A-T with two hydrogen bonds has a very similar value of β_{max} of 0.72 Å^{-1}. However, the two-hydrogen-bonded wobble base pair (G-T) has a significantly larger value of 0.79 Å^{-1}. This approximately 10% increase in the decay constant reduces its estimated maximum conductance by a factor of ~2–3 compared to the others.

An interesting comparison occurs with 2AA-T (3HB) and A-T (2HB). Figure 4(d) shows that the band gap of 2AA-T decreases by 15% (ΔE_G=0.45 eV) compared to A-T, while the decay constant decreases only by 1.5% ($\Delta\beta_{max}$ =0.01 Å^{-1}) (Table III). A partial explanation why β_{max} decreases so little with the increased number of hydrogen bonds in 2AA-T is because the hydrogen-bond distances increase in 2AA-T compared to A-T.

IV. FERMI-LEVEL ALIGNMENT

The tunneling conductance of a molecule of length L is controlled by the exponential decay constant $\beta(E)$ ($G \approx G_0 e^{-\beta(E)L}$). It is important to know the energy E of the tunneling electrons. Electrons that contribute to the current are those with energy near the Fermi level of the metal. Therefore it is important to know how the Fermi level of the metal is aligned relative to the molecular energy levels. If the Fermi level is aligned in the middle of the band gap, the decay constant becomes maximum, which yields a low conductance. If the Fermi level lies near the HOMO or the LUMO, the decay constant decreases dramatically with a resulting conductance increase.

We perform plane-wave [46] DFT-LDA pseudopotential calculations of the electronic structure to determine the Fermi-level alignment. The Fermi-level alignment is determined from the electronic density of states (DOS) projected onto base-pair atoms. A supercell is used which is periodic both in the direction of the molecular axis and in the perpendicular directions. The systems constructed are gold/molecule/gold constructs with the molecule being G-C, A-T, G-T, or 2AA-T base pairs. The gold slabs are (111), six layers thick, and 3×3 in plane. The Au-Au bond length is 2.885 Å. The base pair is thiolated after removing a hydrogen atom on both ends. The sulfur atom is positioned at the on-top site of the (111) gold slabs with Au-S distance of 2.42 Å [47]. The on-top site contact (rather than the hollow site) was used to prevent base-pair hydrogen atoms from being too close to the Au plane. The molecular axis of base pair is inclined rather than directly perpendicular to the Au plane [48]. For example, G-C base pair is oriented to have Au-S-C angles at either end of 120° and 140°.

Figure 5 shows the DOS projected onto elements (C, N, and O) on each nucleobase for G-C, A-T, G-T, and 2AA-T base pairs and the sulfur atom. The Fermi level of the metal is adjusted to be zero energy in the figure. The band gap of the G-C base pair appears to be about 3.34 eV, which is larger by 0.64 eV than the band gap obtained in Sec. III [Fig. 4(a)] using a different code [43] for a periodic molecule with no metal contacts (Fig. 3). We have checked that the difference is due to the metal contacts and not the plane-wave code used. The band gaps for G-C, A-T, G-T, and 2AA-T base pairs are all similar (~3.2–3.4 eV).

The projected DOS shows that the HOMO broadens due to coupling with the metal levels. The Fermi level is found to be aligned very close to the peak of the HOMO level for all base pairs. It is particularly close for the 2AA-T base pair (only 0.04 eV above the HOMO). Alignment of the Fermi level of gold to be near the HOMO indicates that the conductance of base pairs will be much higher than the minimum conductance estimated in Sec. III using β_{max}. From these Fermi-level alignments, the complex band structure (Fig. 4) can be used to roughly determine the decay constant at the Fermi level, $\beta(E_F)$. The estimate becomes less accu-

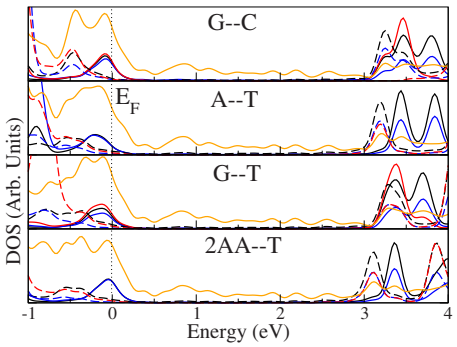

FIG. 5. (Color online) Averaged projected DOS per atom for G-C, A-T, G-T, and 2AA-T. The projected DOSs onto carbon, nitrogen, oxygen, and sulfur atoms are represented in black, blue, red, and orange colors. Solid and broken lines are the projected DOSs onto atoms on purines (G, A, and 2AA) and pyrimidines (C and T), respectively. The HOMO is dominated by the orbitals on purine (guanine for G-C and G-T, adenine for A-T, and diaminoadenine for 2AA-T), and the LUMO is dominated by the orbitals on pyrimidine (cytosine for G-C and thymine for G-T, A-T, and 2AA-T).

rate because the broadening of the HOMO level is not taken into account, which becomes more important as the Fermi level approaches the HOMO. These estimates are listed in Table III. The sensitive dependence of β on energy when the energy is not near the midgap gives rise to significant differences in β between base pairs (0.30–0.48 Å^{-1}). The reduction in β increases the conductance G; the conductance increases by a factor of ~20 (for A-T) to ~200 (for 2AA-T) compared to the minimum computed conductance. This clearly shows the importance of Fermi-level alignment and its dependence on metal contact.

There is a difference in $\beta(E_F)$ between base pairs with three hydrogen bonds (G-C and 2AA-T) and two-hydrogen-bonded base pairs (A-T and G-T). For example, $\beta(E_F)$ of G-T is higher than $\beta(E_F)$ of 2AA-T by 0.18 Å^{-1}, which results in the lower conductance for G-T by a factor of 9 compared to 2AA-T. On the other hand, whether the base pair is the Watson-Crick complementary base pair (A-T) or the wobble base pair (G-T) does not seem to affect the conductance—we obtained almost the same conductance for A-T as G-T. These results are confirmed from the *I-V* calculation as we will explain in Sec. V.

The projected density of states shows that the HOMO and the LUMO are localized onto different nucleobases in all four base pairs. For G-C, the HOMO is dominated by the orbitals on guanine, while the LUMO is dominated by the orbitals from cytosine. For A-T and 2AA-T, the HOMO is localized onto adenine or 2AA, while the LUMO is localized onto thymine. For G-T, the HOMO and the LUMO are localized onto guanine and thymine, respectively. These findings are in line with the findings in Fig. 2(a). Similar localization was obtained for the periodic base pairs of G-C, A-T, G-T, and 2AA-T without the metal contact.

Yanov and Leszczynski [20] found some similarity with these results for the A-T base pair sandwiched between the metal electrodes. They showed that the HOMO is localized onto adenine and the LUMO onto thymine. However, the Fermi-level alignment was significantly different from what is obtained here. Their calculation, using semiempirical nonequilibrium Green's function, showed that the Fermi level is aligned near the LUMO rather than the HOMO. Presumably, this difference occurs because of charge redistribution at the interface not captured due to a lack of self-consistency in the semiempirical calculations.

V. *I-V* CALCULATION

Ballistic transport theory is used to determine the *I-V* characteristics, specifically the conductance of each base pair. Electron conductance is viewed as a quantum-mechanical transmission of electrons through a barrier [41,49–53]. Our implementation is Green's function based, and the current is given by the integration of the transmission function over the energy within the Fermi level of the left and the right metal electrodes under the bias,

$$I = \frac{2e}{h}\int_{\mu_R}^{\mu_L} T(E)dE. \tag{1}$$

The heart of the matter is the transmission function $T(E)$, and μ_L and μ_R are the Fermi energies of the left and right electrodes under the applied bias. The transmission function is given by

$$T(E) = \mathrm{tr}(\Gamma_L G_M \Gamma_R G_M^\dagger), \tag{2}$$

where $\Gamma_{L(R)}$ is the spectral density of states of the left and the right electrodes,

$$\Gamma_L = i(\Sigma_L - \Sigma_L^\dagger), \tag{3}$$

and Σ is the "self-energy,"

$$\Sigma_L(E) = (ES_{LM} - H_{LM})^\dagger G_L^0(E)(ES_{LM} - H_{LM}). \tag{4}$$

Here G_M is Green's function for the molecule, and S_{LM} and H_{LM} are the overlap and Hamiltonian coupling matrix elements between the left contact and the molecule.

Complete details of our computational and theoretical strategy are described in Refs. [41,54]. The method uses supercells containing metallic (gold) slabs and the molecule. A block recursion method [41,55] is used to transform the finite gold slabs into semi-infinite bulk electrodes. All interactions such as molecule-metal and molecule-molecule are obtained self-consistently at zero bias. The bias is applied by assuming a symmetric drop across each of two metal/molecule interfaces.

The electronic structure is determined by a local-orbital description. The SIESTA code [56] uses localized pseudoatomic orbitals (PAOs) as the basis in the DFT local-density approximation with pseudopotentials. In this work, double-zeta basis plus polarization orbitals (DZP) was used for all atoms except Au [single-zeta basis plus polarization orbitals (SZP)]. The supercell system is exactly the same as the one used in the projected-density-of-states calculation in Sec. IV.

Figure 6 shows the transmission functions for G-C, A-T, G-T, and 2AA-T base pairs. All the curves are adjusted so that the Fermi energy is defined to be zero energy. The Fermi level is aligned very close to the HOMO in all cases in agreement with plane-wave results described earlier. The band gap

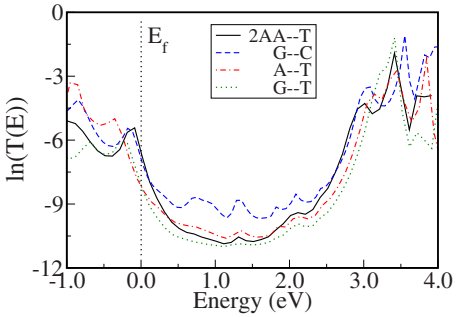

FIG. 6. (Color online) Transmission function as a function of energy for G-C, A-T, G-T, and 2AA-T base pairs. The Fermi level is defined to be zero energy in the figure. The transmission probability at the Fermi level is higher for G-C and 2AA-T than for A-T and G-T. The Fermi level is aligned near the HOMO in all cases.

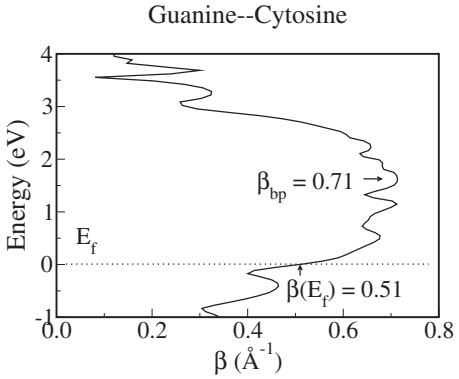

FIG. 7. The decay parameter $\beta(E)$ obtained from the transmission function for the G-C base pair ($\beta(E)=-\ln[T(E)]/L$). The semielliptical curve shows that the decay constant is 0.71 Å^{-1} at the branch point and 0.51 Å^{-1} at the Fermi level.

also shows good agreement with the plane-wave basis-set calculation (e.g., $E_G=3.2$ eV using local orbitals and 3.3 eV using plane-wave basis set for G-C). The transmission function for the four base pairs clearly shows how complex the situation is. Near the metal Fermi level, the base pairs with three hydrogen bonds (G-C and 2AA-T) have higher transmission probability than those with two hydrogen bonds (A-T and G-T). This agrees with the conductance estimate obtained using $\beta(E_F)$ in Sec. IV. At the Fermi energy, A-T and G-T show almost the same transmission probability, and 2AA-T has slightly higher $T(E)$ than G-C, which is also consistent with the results in Sec. IV.

The situation in the midgap region yields different results. Here G-T has the smallest transmission function, again in agreement with the CBS results (Fig. 4). What does not agree is that the transmission function for G-C base pair is significantly enhanced compared to 2AA-T and A-T. We have no simple explanation for this enhancement.

The current-voltage (I-V) curves for G-C, A-T, G-T, and 2AA-T are all linear for small voltage region between −0.1 and +0.1 V. We focus only on small voltages—in a DNA recognition or sequencing device in water, small voltages are necessary to ensure that electrochemistry does not take place. As we can expect from the transmission function, G-C and 2AA-T have higher conductance than A-T and G-T. The current is higher for 2AA-T than G-C, and is almost the same for A-T and G-T, which agrees with result of the estimated conductance using $\beta(E_F)$ in Sec. IV. The conductance for each base pair was obtained from the slope of linear part of I-V curve, and is listed in Table III. Although the conduction trends among base pairs shows agreement between the I-V calculation and the complex-band-structure estimates, the absolute value of the conductance shows discrepancy. The conductance estimate from $\beta(E_F)$ predicts a higher conductance by about an order of magnitude. As discussed above, most of this discrepancy is due to the sharp drop in β as E_F approaches the HOMO (energy zero in the CBS curves), while the effective β contained in the transmission function is not reduced as dramatically because of the HOMO level broadening. Additionally, the CBS conductance estimate does not consider the effect of metal-molecule contact interaction, or on details of the contact geometry.

From the information of transmission probability we obtain the approximate decay function $\beta(E)$ [$\beta=-\ln T(E)/L$]. For L we used the distance between the two sulfur atoms. The $\beta(E)$ curve shown in Fig. 7 for G-C gives the maximum value of about 0.71 Å^{-1}. It is remarkable that this is the same value as obtained from the CBS in Sec. III ($\beta_{max}=0.70$ Å^{-1}). Figure 7 also shows $\beta(E_F)$ using the Fermi-level alignment from the transmission function and it is 0.51 Å^{-1}. This value of $\beta(E_F)$ is higher than the value obtained using the CBS and explains the difference in conductances between the I-V results and the CBS (Table III) [$\beta(E_F)=0.35$ Å^{-1}]. The origin of this difference is clear. The complex band structure has a well-defined "HOMO band" at which β goes to zero. For the metal/molecule/metal sandwich, the HOMO level is broadened out in energy, mixing with many gold levels and becomes ill defined. Therefore β is not allowed to drop to zero, making the metal/molecule/metal conductance far less than the simple CBS result. In some sense, the significant difference between the conductance values from the CBS and the metal/molecule/metal system is because of the "accidental" closeness of the Fermi-level alignment with the HOMO. Additionally, it may seem peculiar that the metal/molecule/metal I-V method produces such a low conductance (compared to G_0) as the Fermi level approaches the HOMO. We believe that the origin of this is that the HOMO wave function is inhomogeneously distributed over the base pair.

VI. CONDUCTANCE OF DEOXYNUCLEOSIDE-NUCLEOBASE COMPLEX

The complex band structure and I-V calculation for DNA base pairs suggest that the number of hydrogen bonds plays a role in determining the conductance of base pairs—more hydrogen bonds lead to noticeably higher conductance. This result suggests the feasibility of identifying DNA bases by reading the electrical signal of hydrogen-bonded base pairs. Recently He *et al.* [16] measured the decay of current with distance when a nucleobase-functionalized STM probe is pulled away from nucleoside monolayers. They found that the current decays slowly when the hydrogen bond is formed between G-C base pair (guanine-functionalized STM tip is used on a deoxycytidine monolayer) compared to G-T base

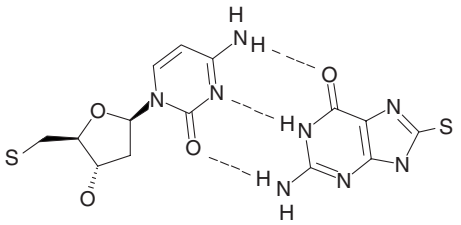

FIG. 8. Schematic diagram of deoxycytidine-guanine. The hydrogen atoms on both ends are replaced by sulfur to make contacts with the gold electrodes for *I-V* calculation.

pair (guanine-functionalized tip on deoxythymidine monolayer). We performed *I-V* calculation for hydrogen-bonded base pairs with deoxyribose attached to one nucleobase (nucleoside-base complex). The four nucleoside-base systems are deoxycytidine-guanine, deoxythymidine-diaminoadenine, deoxythymidine-adenine, and deoxythymidine-guanine. Figure 8 shows the schematic diagram of the thiolated deoxycytidine-guanine used in an *I-V* calculation where the two S atoms are attached to gold and are similar to the recent STM experiment by He *et al.* [16].

First we obtained the optimized structure of deoxynucleoside by energy minimization using DFT with B3LYP. It then was aligned with the nucleobase (optimized using the same method) in a way that two nucleobases become coplanar and have proper hydrogen-bond lengths determined by geometry optimization of base pairs.

The *I-V* calculations were performed with small bias (± 0.1 V). It was found that deoxyribose reduces the conductance substantially. In fact, the conductance is no longer roughly proportional to the number of hydrogen bonds. Table IV shows a summary of the *I-V* determined conductances of base pairs and nucleoside-base complexes. There is a significant decrease in the conductance when the deoxyribose is attached to the base, which is expected because the deoxyribose and base lies almost perpendicular to each other rather than being in plane after geometry optimization. More importantly, it clearly shows that the number of hydrogen bonds in base pairing of a nucleoside-nucleobase pair is not a decisive factor that determines the conductance. The slight shifts of the Fermi-level alignment relative to the HOMO is just as important as the number of hydrogen bonds when the electrical resistance becomes high. This result indicates that it becomes more difficult to identify DNA for sequencing from only the transverse conductance of DNA tethered to the metal electrode via hydrogen bonding with a probe nucleobase attached to a second contact.

TABLE IV. The conductances in nS for the base pairs ($G_{B\text{-}B}$) and the nucleoside-base complex ($G_{NS\text{-}B}$) determined by an *I-V* calculation [Eq. (1)]. Four base pairs are considered, and the number of hydrogen bonds for each base pair is indicated in parenthesis. For base pairs three-hydrogen-bonded base pairs (G-C and 2AA-T) have higher conductance by a factor of 4–5 than two-hydrogen-bonded base pairs (A-T and G-T). Attaching deoxyribose reduces the conductance significantly, and conductances do not correlate well with the number of hydrogen bonds.

	$G_{B\text{-}B}$ (nS)	$G_{NS\text{-}B}$ (nS)
G-C (3HB)	83.8	0.96
2AA-T (3HB)	119	1.43
A-T (2HB)	22.2	1.62
G-T (2HB)	23.7	0.54

TABLE V. The decay constants near midgap (β_{max}) and the estimated conductances (G) for different numbers of hydrogen bonds (N_{HB}) within the DNA base pair. The conductance decreases as the number of hydrogen bonds decreases but the decrease is less than linear.

	G-C	G-C	A-T	A-T	G-T
N_{HB}	3	1	2	1	2
β_{max} (Å^{-1})	0.70	0.76	0.72	0.76	0.79
G_{min} (nS)	9.82	4.83	7.83	5.00	3.70

VII. EFFECT OF THE NUMBER OF HYDROGEN BONDS ON CONDUCTANCE

The conductance is affected by the relative alignment of the HOMO and metal Fermi level, and also by the number of hydrogen bonds within the base pair. We seek a direct determination of just the dependence of the conductance on the number of hydrogen bonds connecting a base pair. To do this, we computed the complex band structure for modified base pairs where the modification involves removing hydrogen bonds. Hydrogen bonds are removed by rotating the NH_2 out of the bonding plane. For the G-C base pair, the -NH_2 donor groups in cytosine and guanine are rotated by 90° about C-N axis. This moves the H atom far away (e.g., 1.7–1.9 Å$\rightarrow$2.7–2.8 Å) from the acceptor on the other base. We assume that this causes the hydrogen bond between NH$\cdots$O to be broken.

As a measure of the effectiveness of hydrogen-bond tunneling, we inspect the decay constant β for the G-C base pair at its maximum value in the band-gap region (β_{max}), and estimate the conductance using $G=G_0e^{-\beta_{max}L}$. Table V shows how the decay constant and the conductance vary when both of the -NH_2 groups in cytosine and guanine were rotated. Thus three hydrogen bonds are reduced to just one. There is only a modest change in β_{max} and it increases by only 8% when two hydrogen bonds are removed. However, since the conductance depends exponentially on β, the conductance decreases by a factor of 2.0. We also changed the number of hydrogen bonds in A-T base pair by rotating the -NH_2 group in adenine. The conductance decreased by a factor of 1.6 when only one hydrogen bond remains compared to when there are two hydrogen bonds in base pair. Of course, it is expected that the base pair becomes less conductive as the number of hydrogen bonds is reduced, but the conductance reduction is much smaller than linear.

VIII. ISOLATING β OF A HYDROGEN BOND

The decay constant obtained from the complex band structure is the overall decay constant for a unit cell, which

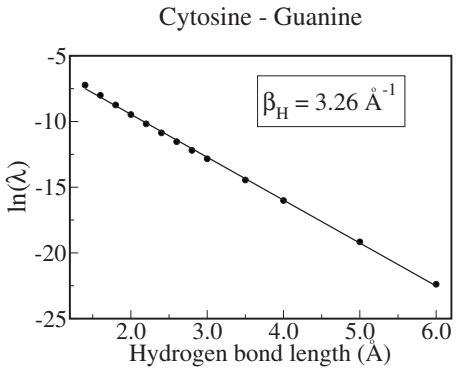

FIG. 9. Plot of ln λ vs L_H for the G-C base pair, where λ is the decay per cell of the tunneling probability and L_H is the central hydrogen-bond distance. The base pair is rigidly moved apart to change L_H.

includes both the covalent bond and the hydrogen bond. We have found that this "global decay" has a maximum of 0.7–0.8 $Å^{-1}$ for base pairs. How can we isolate the contribution from the hydrogen bond itself? There is no simple solution to this, but a "differential β" gives a partial answer. Here we change the hydrogen bond-length between a base pair to obtain insight into the decay constant of the hydrogen bond itself. The simplest assumption for the relationship between the overall decay constant ($\beta_{overall}$) of the whole system with length L and the decay constant of each component (β_i) with length L_i would be the linear relationship, $\lambda = e^{-\beta_{overall}L} = \exp(-\Sigma_i \beta_i L_i) = e^{-\beta_H L_H} e^{-\beta_C L_C}$ (the subscripts H and C indicate the hydrogen bond and the covalent bond, respectively). Here λ is the decay factor from cell to cell determined by the complex k vector that is the output from CBS method, $\lambda = |e^{ikL}|^2$. By taking the natural logarithm and differential with respect to L_H, we define β_H as $d(\ln \lambda)/dL_H = -\beta_H$. This simple, but approximate, result means that the decay constant for just the hydrogen bond itself can be obtained by from λ by varying the hydrogen-bond distance (L_H) while keeping all the other bond lengths the same.

Figure 9 shows the result of λ versus hydrogen-bond distance. We extend all hydrogen-bond lengths uniformly by rigidly moving the two bases away or toward each other. The hydrogen-bond length in the Fig. 9 is the central N-H-N bond length. It is seen that ln λ decreases linearly as the hydrogen-bond distance increases for the G-C base pair. It gives $\beta_H = |\text{slope}| = 3.3$ $Å^{-1}$, which is far higher than $\beta_{overall}$ (=0.70 $Å^{-1}$). The higher value of β_H compared to $\beta_{overall}$ indicates that the hydrogen-bond tunneling is less conductive than the "through-bond" tunneling within the molecule as we expect. Since β_H is so large, fluctuations around the equilibrium hydrogen-bond lengths that occur in solution will produce larger current variations than those expected from $\beta_{overall}$. The analysis was repeated for the A-T base pair, which contains two hydrogen bonds. The value of β_H obtained from the |slope| of ln λ vs L_H plot was lower in the A-T base pair (2.6 $Å^{-1}$) than in G-C base pair (3.3 $Å^{-1}$).

IX. CONCLUSION

In this paper we investigated the electron-tunneling property of different base pairs (G-C, A-T, G-T, and 2AA-T) using the methods of complex band structure and of Green's-function scattering theory for I-V characteristics. The projected density of states using both plane-wave basis set and local orbitals shows that the Fermi level is aligned very close to the HOMO in all cases, and the HOMO and the LUMO are localized onto orbitals on purine and pyrimidine, respectively. Conductances estimated from the decay constant of tunnel current at the Fermi level and from the I-V calculation indicate that three-hydrogen-bonded base pairs (G-C and 2AA-T) are more conductive than two-hydrogen-bonded base pairs (A-T and G-T) by a factor of 4–10. However, the conductance of nucleoside-base complex decreases significantly compared to the conductance of base pairs, and it becomes difficult to distinguish the base pairing by measuring the conductance of nucleoside-base complex.

As more hydrogen bonds are formed between the DNA bases, higher conductance for the same base pair was observed. The decay constant β for a unit cell of base pair increases as the hydrogen-bond distance increases, resulting in a linear relationship between the logarithm of the decay rate (λ) of the tunneling probability and the hydrogen-bond distance.

ACKNOWLEDGMENTS

We are pleased to acknowledge a close and fruitful collaboration with the experimental sequencing team including J. He, L. Lin, Q. Spadola, Z. Xi, Q. Fu, S. Chang, S. Huang, P. Pang, D. Cao, F. Liang, H. Liu, K. Reinhart, P. Zhang, and S. Lindsay. We acknowledge support from the DNA Sequencing Technology Program of the National Human Genome Research Institute (Grant No. 1 R21 HG004378-01).

[1] V. Bhalla, R. P. Bajpai, and L. M. Bharadwaj, EMBO Rep. **4**, 442 (2003).
[2] M. Zwolak and M. Di Ventra, Rev. Mod. Phys. **80**, 141 (2008).
[3] H.-W. Fink and C. Schönenberger, Nature (London) **398**, 407 (1999).
[4] D. Porath, A. Bezryadin, S. de Vries, and C. Dekker, Nature (London) **403**, 635 (2000).
[5] F. D. Lewis, X. Liu, J. Liu, S. E. Miller, R. T. Hayes, and M. R. Wasielewski, Nature (London) **406**, 51 (2000).
[6] B. Xu, P. Zhang, X. Li, and N. Tao, Nano Lett. **4**, 1105 (2004).
[7] Y. A. Berlin, A. L. Burin, and M. A. Ratner, J. Am. Chem. Soc. **123**, 260 (2001).
[8] F. C. Grozema, Y. A. Berlin, and L. D. A. Siebbeles, J. Am. Chem. Soc. **122**, 10903 (2000).
[9] M. Akeson, D. Branton, J. K. Kasianowicz, E. Brandin, and D. W. Deamer, Biophys. J. **77**, 3227 (1999).
[10] D. W. Deamer and M. Akeson, Trends Biotechnol. **18**, 147 (2000).

[11] D. W. Deamer and D. Branton, Acc. Chem. Res. **35**, 817 (2002).
[12] J. K. Kasianowicz, E. Brandin, D. Branton, and D. W. Deamer, Proc. Natl. Acad. Sci. U.S.A. **93**, 13770 (1996).
[13] M. Zwolak and M. Di Ventra, Nano Lett. **5**, 421 (2005).
[14] R. Zikic, P. S. Krstić, X.-G. Zhang, M. Fuentes-Cabrera, J. Wells, and X. Zhao, Phys. Rev. E **74**, 011919 (2006); X.-G. Zhang, P. S. Kristić, R. Zikić, J. C. Wells, and M. Fuentes-Cabrera, Biophys. J. **91**, L04 (2006).
[15] T. Ohshiro and Y. Umezawa, Proc. Natl. Acad. Sci. U.S.A. **103**, 10 (2006).
[16] J. He, L. Lin, P. Zhang, and S. M. Lindsay, Nano Lett. **7**, 3854 (2007).
[17] J. He, L. Lin, P. Zhang, Q. Spadola, Z. Xi, Q. Fu, and S. Lindsay, Nano Lett. **8**, 2530 (2008); J. He, L. Lin, H. Liu, P. Zhang, M. Lee, O. F. Sankey, and S. M. Lindsay, Nanotechnology **20**, 075102 (2009).
[18] C. R. Cantor and P. R. Schimmel, *Biophysical Chemistry* (Freeman, San Francisco, 1980).
[19] 2AA-T is obtained by replacing one hydrogen atom on adenine by -NH_2-, so that an additional hydrogen bond (NH$\cdots$O) is formed between 2AA and T.
[20] I. Yanov and J. Leszczynski, Int. J. Quantum Chem. **96**, 436 (2004).
[21] S. S. Mallajosyula and S. K. Pati, J. Phys. Chem. B **111**, 11614 (2007).
[22] L. A. Jauregui and J. M. Seminario, IEEE Sens. J. **8**, 803 (2008).
[23] J. K. Tomfohr and O. F. Sankey, Phys. Rev. B **65**, 245105 (2002).
[24] M. W. Schmidt, K. K. Baldridge, J. A. Boatz, S. T. Elbert, M. S. Gordon, J. H. Jensen, S. Koseki, N. Matsunaga, K. A. Nguyen, S. J. Su, T. L. Windus, M. Dupuis, and J. A. Montgomery, J. Comput. Chem. **14**, 1347 (1993).
[25] S. Tsuzuki and H. P. Lüthi, J. Chem. Phys. **114**, 3949 (2001).
[26] K. Brameld, S. Dasgupta, and W. A. Goddard III, J. Phys. Chem. B **101**, 4851 (1997).
[27] C. F. Guerra, F. M. Bickelhaupt, J. G. Snijders, and E. J. Baerends, Chem.-Eur. J. **5**, 3581 (1999).
[28] J. Bertran, A. Oliva, L. Rodríguez-Santiago, and M. Sodupe, J. Am. Chem. Soc. **120**, 8159 (1998).
[29] J. Šponer, P. Jurečka, and P. Hobza, J. Am. Chem. Soc. **126**, 10142 (2004).
[30] J. Šponer, J. Leszczynski, and P. Hobza, J. Phys. Chem. **100**, 1965 (1996).
[31] Y. Mo, J. Mol. Model. **12**, 665 (2006).
[32] T. van der Wijst, C. F. Guerra, M. Swart, and F. M. Bickelhaupt, Chem. Phys. Lett. **426**, 415 (2006).
[33] R. S. Fellers, D. Barsky, F. Gygi, and M. Colvin, Chem. Phys. Lett. **312**, 548 (1999).
[34] W. Saenger, *Principles of Nucleic Acid Structure* (Springer, Berlin, 1984), pp. 123 and 124, and references therein.
[35] C. Lee, W. Yang, and R. G. Parr, Phys. Rev. B **37**, 785 (1988); A. D. Becke, J. Chem. Phys. **98**, 5648 (1993); P. J. Stephens, F. J. Devlin, C. F. Chabalowski, and M. J. Frisch, J. Phys. Chem. **45**, 11623 (1994).
[36] D. Voet, W. B. Gratzer, R. A. Cox, and P. Doty, Biopolymers **1**, 193 (1963).
[37] L. B. Clark and I. Tinoco, Jr., J. Am. Chem. Soc. **87**, 11 (1965).
[38] C. A. Sprecher and W. C. Johnson, Biopolymers **16**, 2243 (1977).
[39] L. B. Clark, J. Phys. Chem. **94**, 2873 (1990).
[40] L. Hawke, G. Kalosakas, and C. Simserides, e-print arXiv:0808.3984.
[41] J. Tomfohr and O. F. Sankey, J. Chem. Phys. **120**, 1542 (2004).
[42] D. Vanderbilt, Phys. Rev. B **41**, 7892 (1990).
[43] F. Picaud, A. Smogunov, A. Dal Corso, and E. Tosatti, J. Phys.: Condens. Matter **15**, 3731 (2003); S. Baroni, A. D. Corso, S. de Gironcoli, and P. Giannozzi, http://www.pwscf.org
[44] B. Xu and N. J. Tao, Science **301**, 1221 (2003).
[45] J. K. Tomfohr and O. F. Sankey, Phys. Status Solidi B **233**, 59 (2002).
[46] The Vienna *Ab initio* Simulation Program (VASP) was developed at the Institut für Theoretiche Physik of the Technische Universität Wien: G. Kresse and J. Furthmüller, Comput. Mater. Sci. **6**, 15 (1996); G. Kresse and J. Hafner, Phys. Rev. B **47**, 558 (1993); G. Kresse and J. J. Furthmüller, *ibid.* **54**, 11169 (1996).
[47] H. Kondoh, M. Iwasaki, T. Shimada, K. Amemiya, T. Yokoyama, T. Ohta, M. Shimomura, and S. Kono, Phys. Rev. Lett. **90**, 066102 (2003).
[48] G. K. Ramachandran, J. K. Tomfohr, J. Li, O. F. Sankey, X. Zarate, A. Primak, Y. Terazono, T. A. Moore, A. L. Moore, D. Gust, L. A. Nagahara, and S. M. Lindsay, J. Phys. Chem. B **107**, 6162 (2003).
[49] Y. Imry and R. Landauer, Rev. Mod. Phys. **71**, S306 (1999).
[50] R. Landauer, J. Phys.: Condens. Matter **1**, 8099 (1989).
[51] S. Datta, *Electronic Transport in Mesoscopic Systems* (Cambridge University Press, Cambridge, England, 1995).
[52] M. Büttiker, Y. Imry, R. Landauer, and S. Pinhas, Phys. Rev. B **31**, 6207 (1985).
[53] Y. Xue, S. Datta, and M. A. Ratner, Chem. Phys. **281**, 151 (2002).
[54] J. Li, J. K. Tomfohr, and O. F. Sankey, Physica E **19**, 133 (2003).
[55] P. S. Damle, A. W. Ghosh, and S. Datta, Phys. Rev. B **64**, 201403(R) (2001).
[56] Pablo Ordejón, Daniel Sánchez-Portal, Emilio Artacho, and José M. Soler, and Alberto García, SIESTA code; P. Ordejon, E. Artacho, and J. M. Soler, Phys. Rev. B **53**, R10441 (1996); D. Sánchez-Portal, P. Ordejón, E. Artacho, and J. M. Soler, Int. J. Quantum Chem. **65**, 453 (1997).
[57] A. D. Becke, Phys. Rev. A **38**, 3098 (1988)
[58] J. P. Perdew and Y. Wang, Phys. Rev. B **45**, 13244 (1992); **46**, 6671 (1992).